# Investigation into the Conformational Changes of CTLR Langerin Protonation States

Freie Universität Berlin
Thomas J Leyshon

September 2016

I would like to thank *Stevan Aleskic* and the Keller group for all their help and guidance.

**Abstract**

Langerin, a C-type lectin that resides in Langerhans cell is associated with the process of pattern recognition, uptake and internalization of pathogen such as the HIV and influenza [1]. Revealing the unknown mechanisms of this crucial receptor is key to understanding the human immune system's defence behaviour against such pathogens [2]. Langerin's allosteric binding and release procedure is dictated by two key loops that are positioned around the binding site's cage in which a cell signalling cofactor such as calcium 2+ ion can bind. The affinity of a Ca 2+ ion binding to Langerin is dependent on the protein's structure [3]. The conformational structure of Langerin was compared under various protonation states of amino acid residues surrounding the binding site, H294, E285, E293 and D308. The conformation comparisons showed that E293 protonation appeared to have the greatest effects upon Langerin's flexibility and therefore upon Ca 2+ binding.

# 1 Introduction

Langerhan cells reside in mucus and epidermis layers, they contain organelles called Birbeck granules. Their function is to uptake process microbial antigens to become functional antigen presenting cells . Antigen-presenting cells are important for an efficient adaptive immune response. Antigen presenting cells contribute to immune responses against both intracellular and extracellular pathogens [4].
Great interest has been shown the association of Langerhans cell's with the HIV virus. Langerhan cells located in foreskin and vaginal mucosa are thought to be the initial cellular targets in the sexual transmission of HIV, becoming the sole vector for disseminating throughout the body. Lot de Witte et al. showed evidence that Langerin, the C-type lectin receptor within Langerhan cells are responsible for the prevention of HIV-1 transmission. In Lot de Witte's study HIV-1 was captured by Langerin and internalized into Birbeck granules and degraded (viral clearance)[5]. Inhibition of Langerin also allowed for Langerhans cell infection and subsequent HIV-1 transmission (Lot de Witte). Langerin functions as a scavenger receptor rather than as a transmembrane receptor, restricting T-cell infection by clearing and degrading infectious viral particles. In Lot de Witte's experiment LCs also did not transmit CXCR4 tropic single-round pseudotyped HIV-1 to T cells, this strongly suggests that direct infection of LCs is necessary for transmission.
Langerin binds to an unusually diverse number of endogenous and pathogenic cell surface carbohydrates. Langerin is a Calcium-binding protein, meaning it participates in calcium cell signaling pathways by binding to Ca2+. An enclosure of charged amino acid side chains of the carbohydrate recognition domain (CRD) surrounds a central Ca2+ ion. The CRD is the mediator of interactions and key in regulating the uptake and release of the cargo [6]. Hanske et al. show evidence of important receptor dynamics corresponding to the binding and release of the essential cofactor Ca2+ by the coupled motions of two loops. Valid evidence for an allosteric intra-domain network [1] that regulates the Ca2+ affinity depending on the pH. The pH dependency for both carbohydrate ligands and Ca2+ binding has been seen in CTLRs such as ASGPR, DC-SIGN, and DC-SIGNR [6]. However there is a lack of conformational data on the underlying molecular dynamics of antigen uptake and release. Upon the protonation of the amino acids of the Ca2+ cage the ion is released and carbohydrate interaction are prevented. The central histidine residue of the cage is thought to acts as the pH sensor whose sidechain protonation state controls the Ca2+ affinity [6].
To further understand the underlying receptor dynamics, answers were pursued for the following unknown factors. Which residues have the strongest influence on the Ca2+ release? Is there a pre-ordered structure requested for the Ca2+ binding? How does the protonation of the residues involved in Ca2+ binding influence the coupling between the long, and the short loop? Can the changes in the conformational dynamics of various protonated states be explained in terms of the unsettled hydrogen bond network?

# 2 Experimental Method

The key residues in the Ca2+ cage that were considered in this study consisted of H294, E285, E293 and D308. The table below shows the various protonated states of the investigated residues.

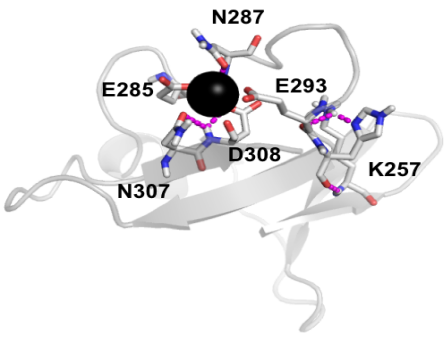


(a) Langerin's Ca2+ binding pocket

| H294 | E285 | E293 | D308 |
|---|---|---|---|
| 0 | 0 | 0 | 0 |
| 1 | 0 | 0 | 0 |
| 0 | 1 | 0 | 0 |
| 0 | 0 | 1 | 0 |
| 0 | 0 | 0 | 1 |
| 1 | 1 | 0 | 0 |
| 1 | 0 | 1 | 0 |
| 0 | 1 | 1 | 0 |
| 1 | 1 | 1 | 0 |
| 1 | 1 | 1 | 1 |

(b) Table of protonated states

Figure 1: Protonated Ca2+ binding pocket residues

[1] regulation of a protein by binding an effector molecule at a site other than the enzyme's active site.

## 2.1 Root Mean Squared Fluctuation (RMSF)

RMSF measures the average distance between the atoms (backbone atoms) of superimposed proteins. The size of the this fluctuation from the defined average position of the atoms provides information on the flexibility and the alternating physical properties of the system [7]. RMSF is mathematically described by

$$RMSF = \sqrt{1/N \sum_{n=1}^{N} |v_i - w_i|^2} \tag{1}$$

where $N$ is the number of equivalent atoms, $v_i - w_i$ is the difference between the average position and the actual position of atom $i$.
The RMSF of the residues surrounding the Ca2+ binding site were taken before and after specific key residue protonations. Through the comparison of RMSF plots between varying protonated residue states, the general trend of the conformation changes can be visualised.

## 2.2 Ramachandran Plots

Ramachandran plots provide a way to identify the energetically allowed regions for backbone dihedral angles, Ψ against Φ of amino acid residues within a protein structure [8]. A dihedral angle is the angle between planes through two sets of three atoms, having two atoms in common. Ramachandran plots also identify the values, or conformations, of the Φ and Ψ angles that are possible for an amino-acid residue within a protein. Left and right handed alpha helices along with beta sheets can be distinguished by particular regions of the plot [8].

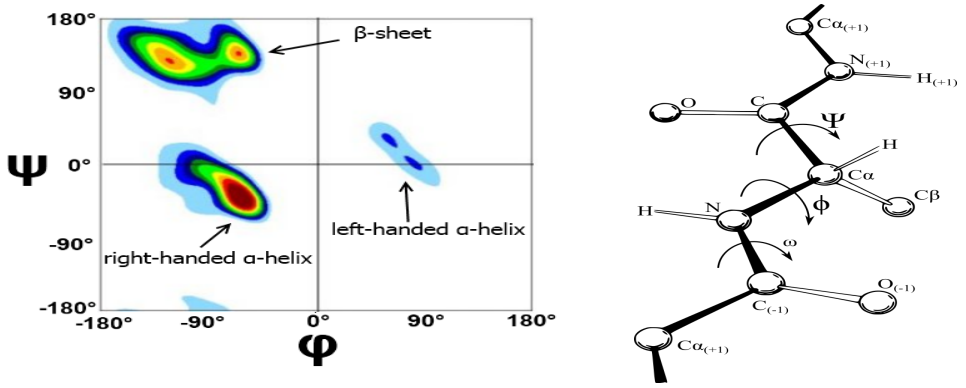


(a) Ramachandran plot

(b) Protein backbone and sidechains

Figure 2: Ramachandran plot showing $\alpha$ helices and $\beta$ sheets, along with protein backbone illustration

These regions are sterically disallowed for all amino acids except glycine. Glycine is unique in that it lacks a side chain. The red regions correspond to conformations where there are no steric clashes, ie. these are the allowed regions namely the alpha-helical and beta-sheet conformations. The yellow areas show the allowed regions if slightly shorter van der Waals radi are used in the calculation, ie. the atoms are allowed to come a little closer together. This produces an additional region which corresponds to the left-handed alpha-helix [9].
Ramachandran plots were made for various combinations of protonation states associated with the 4 key residues within the Ca2+ binding site cage. Through the analysis of Beta sheets and Alpha helices, present in each residue's Ramachandran plots, it was possible for each residue's amino acid type to be identified.
Visual Molecular Dynamics (VMD) software was then used to present the evolution of the residue's amino acid types and overall protein conformation through all the protonation states.

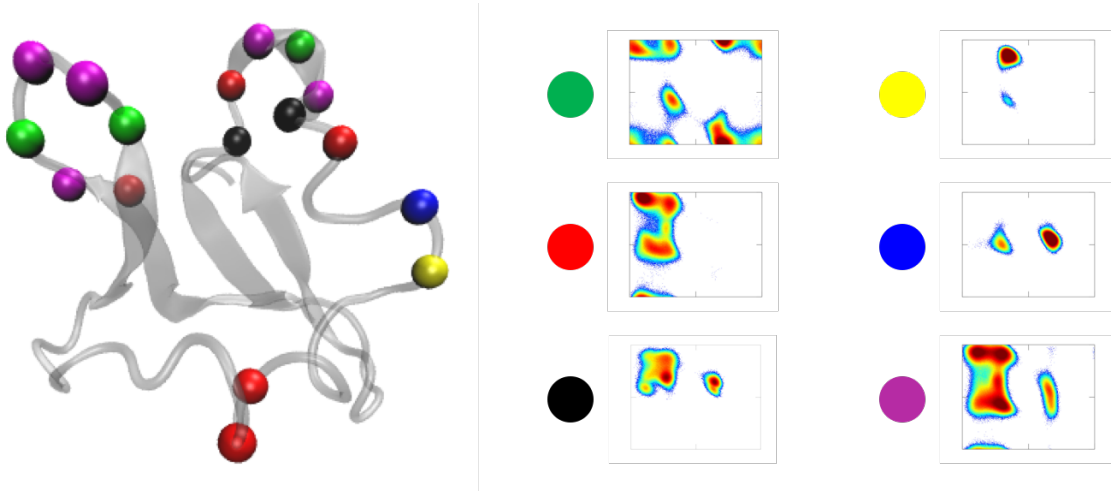

Figure 3: VMD visual representation of Ramachandran plots and amino acid types

Figure 3 shows the VMD visual image used to represent the Ramachandran plots of each residue. Each color represents a different amino acid configuration, categorized by the alpha helices and beta sheets of the residue;

- Black = $\beta$ + Left $\alpha$
- Red = $\alpha + \beta$
- Blue = $\alpha$ + Left $\alpha$
- Green = Glycine
- Yellow = Proline
- Magenta = $\alpha$ + $\beta$ + Left $\alpha$

## 2.3 Conformational Entropy

Conformational entropy was calculated using the backbone dihedral angles, $\Psi$ and side chain rotamers, $\Phi$. These parameters were used to define the degrees of freedom and the possible microstates of the system. Unique combinations of certain structural parameters were identified and each was assigned an energy. The Side-chain conformational entropies were defined over all possible rotameric states using Boltzmann distribution sampling

$$S = -k_b \sum_{i}^{n} p_i ln p_i \tag{2}$$

where $S$ is the conformational entropy, $k_b$ is Boltzmann's constant constant and $p_i$ is the probability of a residue being in rotamer $i$. Protonation of residues causes changes to the conformational entropy associated with each structural combination. It is, therefore, possible to determine the most probable conformational macrostate the protein is to take.

## 2.4 Mutual Information

Mutual information of two random variables is a measure of the amount of information gained about one variable from the other variable [10]. Mathematically mutual information is described by

$$I(X;Y) = \sum_{y} \sum_{x} p(x,y) log(p(x,y)/p(x)p(y)) \tag{3}$$

where $p(x,y)$ is the joint probability distribution function and $p(x)$ and $p(y)$ are the marginal probability distribution functions [10]. It can be seen from this equation that if $x$ and $y$ are independent then I(X;Y) tends to 0.
The mutual dependence data for the protonated states were mapped and visualised using Cytoscape, an open source software platform for visualizing complex networks.

## 2.5 Hydrogen Bond Analysis

Proteins are made out of hundreds of amino acid residues folded into a well defined structure that is stabilized by thousands of interactions [11]. When multiple Hydrogen Bonds connect across multiple amino acid sidechains, they form a Hydrogen Bond Network. The protein structure can be viewed in terms of this Hydrogen Bond Network of contacts (edges) between amino-acid residues (nodes). Individual hydrogen bond provide around $20kJmol^{-1}$ of energy (Fleming and Rose, 2005). The differences in the energy of interaction depend on the geometry of the hydrogen bond. The donor and acceptor must be at the correct distance and angle to be sufficiently strong for a network. The distance between the donor proton and the acceptor (O or N) is always greater than 1.6 and less than 3. The angle between donor-hydrogen-acceptor is greater than or equal to 120° [11]. The critical step of hydrogen bond analysis is to correctly position the backbone hydrogen atoms.

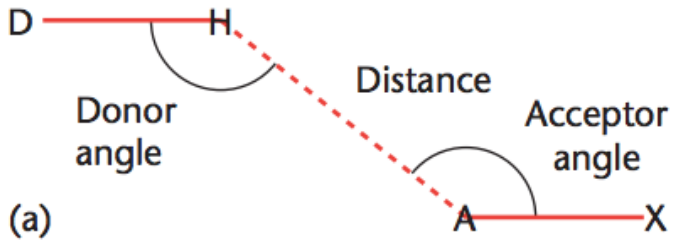


Figure 4: Illustration of a Hydrogen bond's Donor and Acceptor angles

The process used in gromac's hydrogen bond analysis *gmz hbond* determines Hydrogen bonds based on cutoffs for the angle between Hydrogen - Donor - Acceptor and the distance Donor - Acceptor. OH and NH groups are regarded as donors, O is always an acceptor, N is an acceptor by default. Two groups must be specified for analysis, which must be either identical or non-overlapping. All hydrogen bonds between the two groups are analyzed [12].
Hydrogen bonds are an important non-covalent structural force (primarily electrostatic) in molecular systems. They are formed when a single hydrogen atom is effectively shared between the heavy atom that the hydrogen is covalently bonded to (the hydrogen bond donor) and another heavy atom (the hydrogen bond acceptor) [11].

## 2.6 Pka Analysis

When an acid dissociates, it releases a proton to make the solution acidic. Weak acids have both a dissociated state ($A-$) and undissociated state ($AH$). The concentration ratio of both sides is constant given fixed analytical conditions and is referred to as the acid dissociation constant ($Ka$).

$$Ka = \frac{[A^-][H^+]}{AH} \tag{4}$$

$Ka$ therefore expresses the ease in which the acid releases a proton [13]. $pKa$ was introduced as an index to express the acidity of weak acids, where $pKa$ is defined as follows

$$pKa = -\log Ka \tag{5}$$

the smaller the pKa value, the stronger the acid. Strongly altered pKa values are often seen in the active sites of enzymes, to enhance the ability of ionizable residues of acting as nucleophiles, electrophiles or general bases and acids [14]. Our understanding of how changes in environmental pH affect proteins is limited. Changing the pH can modify the protonation state of a residue, which can couple with a conformational change that causes the environment of this residue to change, consequently altering its $pKa$ value [15]. The environment can be greatly altered when the protein changes conformation. As a result, the amino acid will have two different microscopic $pKa$ values. $pKa$ values of amino acid side chains play an important role in defining the pH-dependent characteristics of a protein.
Typically the effects of the protein environment on the amino acid $pKa$ value are divided into pH-independent effects and pH-dependent effects. The pH-independent effects (interactions with permanent charges and dipoles) are added to the model $pKa$ value to give the intrinsic $pKa$ value. The pH-dependent effects cannot be added in the same straight-forward way and have to be accounted for using Boltzmann summation, Tanford Roxby iterations or other methods [16].

Traditionally, the treatment of pH in MD has been limited to setting a fixed protonation state for each titratable residue[2], however there are several problems related to this approach:

- The pKa of a given residue may be unknown [14].
- If the pKa of one residue is similar to the solvent pH, a single protonation state is insufficient to appropriately describe the ensemble of protonation states that will be observed at that pH [14].
- It is not possible to study the coupling between pKa, protonation state and conformation [14].

### 2.7 Allosteric Network

Allosteric communication underlies ligand dependent. It is the phenomenon in which two sites on a single biological molecule are dynamically coupled despite being outside of direct physical interaction range [17]. Allosteric regulation is a modulation of protein function in which binding of ligands (structural excitation) leads to conformational changes. Interacting objects that enhance the protein's activity are referred to as allosteric activators, whereas those that decrease the protein's activity are called allosteric inhibitors [17].
Autocorrelation (ACF) is the correlation of a signal with itself at different points in time. It is a mathematical tool for finding repeating patterns, and is described by

$$ACF = \frac{1}{N}\frac{\sum(Y_i - \bar{Y})(Y_{i+k} - \bar{Y})}{\sum(Y_i - \bar{Y})^2} \tag{6}$$

. Equation 6 was used to distinguish the time dependence as well as the spatial dependence of the conformational changes that cause the coupling of the Langerin protein's long and short loop. The conformational change due to this coupling is greatest between the outer residues of the two loops; residues M60 (short loop) and G290 (long loop).

## 3 Results and Discussion

### 3.1 Results

#### 3.1.1 RMSF

The RMSF plots span across the Langerin's Ca2+ binding pocket, starting at residue 200 and finishing at residue 320 of the Langerin protein. As seen in Figure 5, the comparison of the RMSF of the single protonated states highlights a significant increase in flexibility between residues 280 and 300 that is associated with the protonation of residue E293.

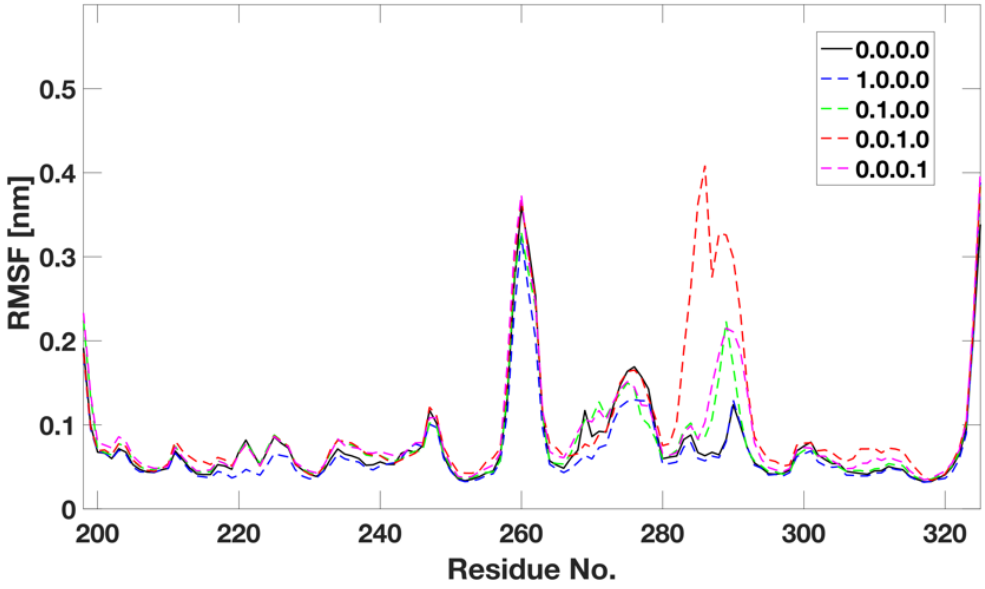


Figure 5: RMSF plot for single protonated states of the Ca2+ binding pocket

[2]any acid that can lose proton(s) in an acid-base reaction

The RMSF plot also indicates the areas most susceptible to conformational change due to protonation, The figures suggest that the most susceptible area is between residue 250 to residue 300.

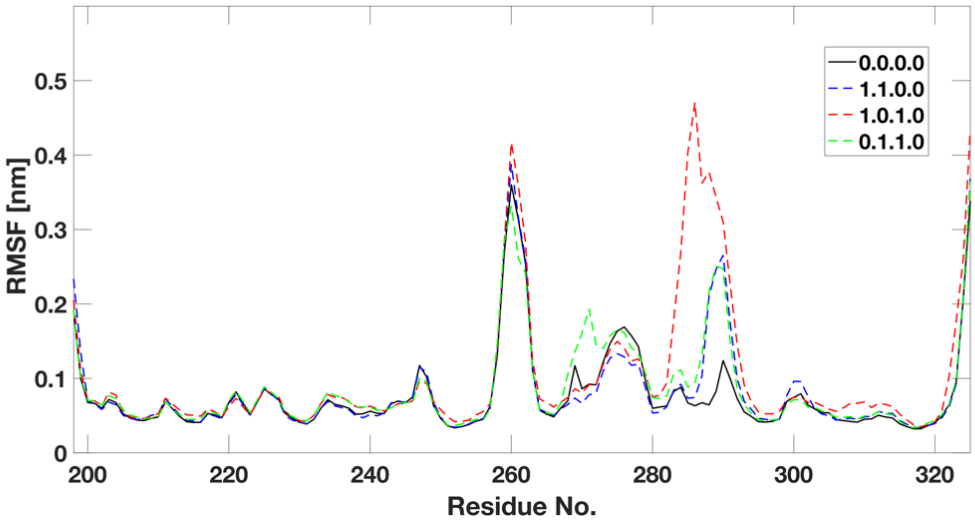


Figure 6: RMSF plot for double protonated states of the Ca2+ binding pocket

Figure 6 shows the RMSF plots for the doubly protonated states. The doubly protonated states are in agreement with the single protonated states. In additional to the protonation of E293 the protonation of H294 showed the same trends in fluctuation and even increased the peak fluctuation compared to the single protonated E293 state. The doubly protonated state of E285 and E293 showed an overall steric hindrance compared to the singly protonated state of E293. However the state also showed an increase in flexibility between residues 265 and 275.

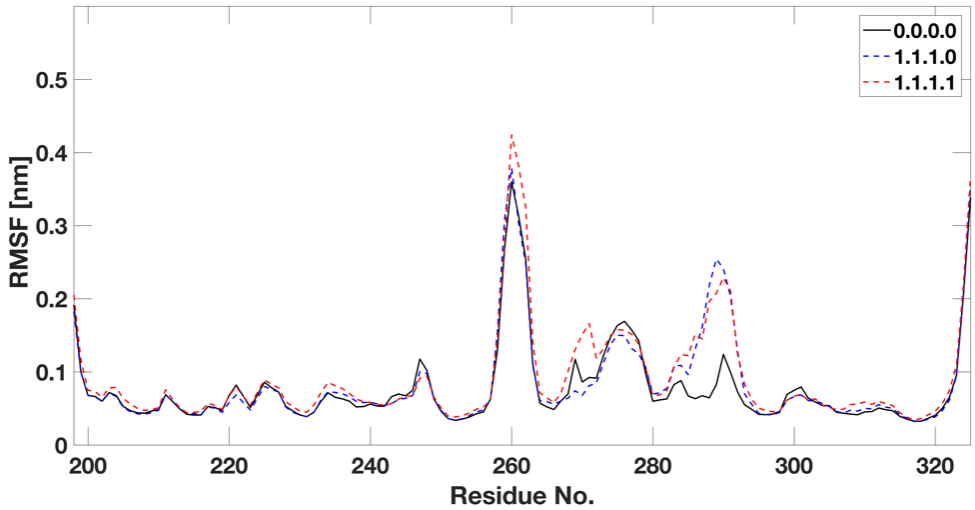


Figure 7: RMSF plot for multiple protonated states of the Ca2+ binding pocket

Figure 7 shows the RMSF plots for the multiple protonated states. It can be seen in the figure that significant steric hindrance is observed, especially between residues 250 and 300. This hindrance results in a substantial loss of flexibility compared to singly protonated states of the same key residues.

### 3.1.2 Ramachandran Plots

Figures 8 and 9 map the ramachandran data of the Langerin protein between residue 250 to 300. It is possible to compare each protonated state with that of the non-protonated state. By consulting the key, figure 3, the

shift in flexibility of each residue due to protonation can be determined by observing the change in the amino acid type.

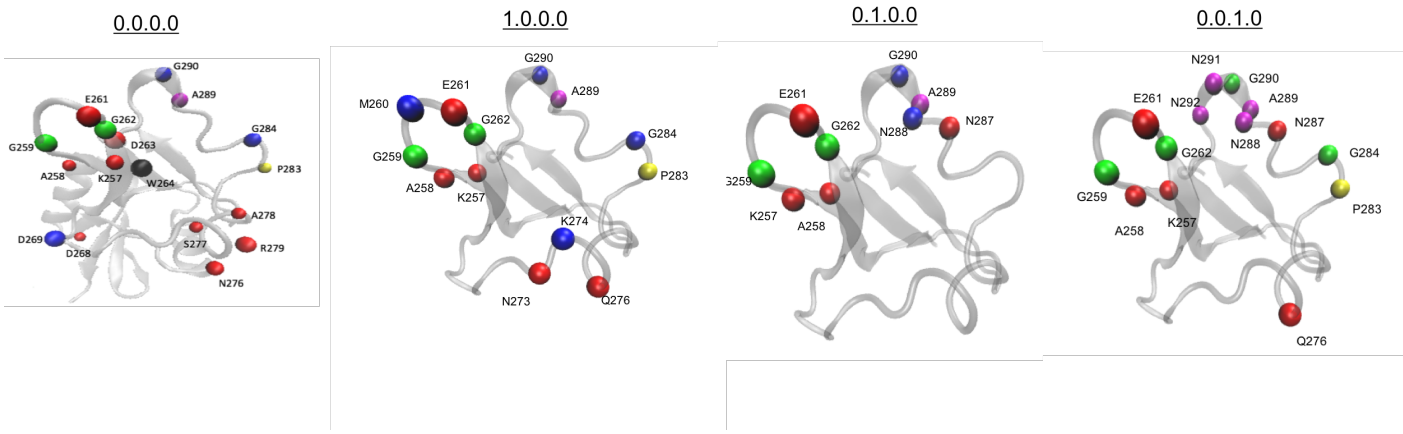


Figure 8: VMD visualization of the residue flexibility due to single protonated states of Ca2+ binding site residues

Figure 8 shows an increase in flexibility of the short loop upon protonation of residue E293. This is determined by the number of magenta residues produced upon E293 protonation. A simultaneous reduction in flexibility occurs upon E293 protonation for the lower region, residues 270 to 280. E285 protonated also shows an increase in short loop flexibility but a significant loss of flexibility in the rest of the residues.
H295 protonation causes little change in binding site flexibility compared to the unprotonated state. E284 protonation shows a slight increase in the long loops flexibility. This increase is indicated with the emergence of N287 and N288. A similar loss of flexibility observed in E293 protonation is observed in the region between 270 and 280.

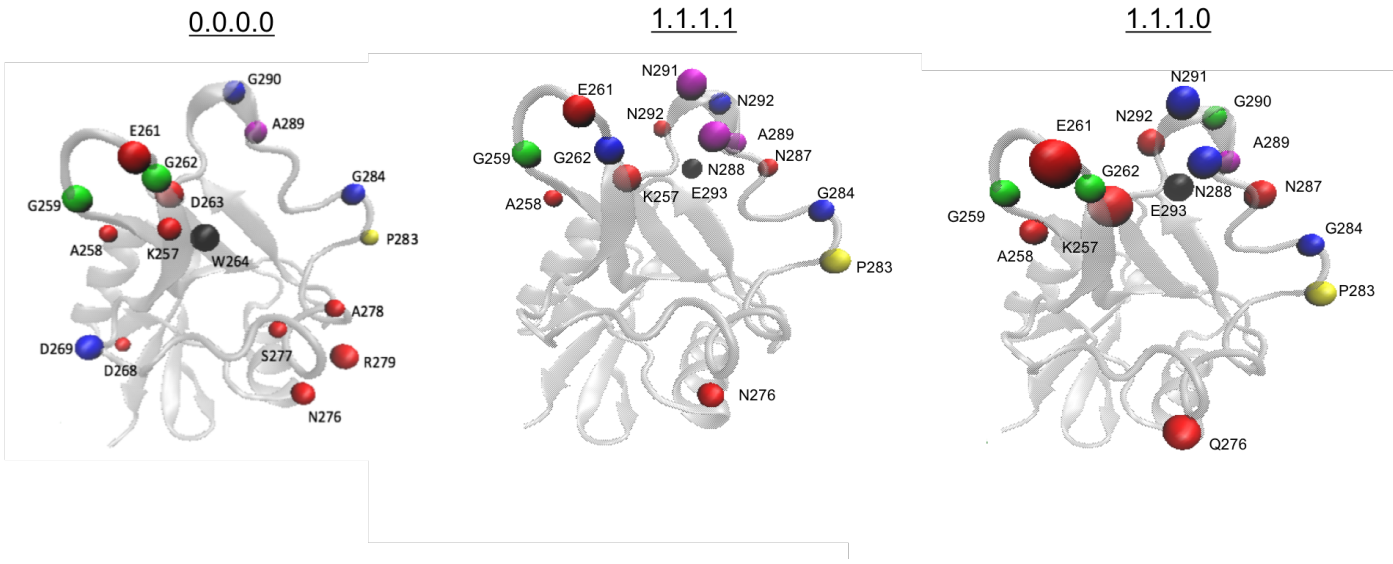


e

Figure 9: VMD visualization of the residue flexibility due to multiple protonated states of Ca2+ binding site residues

Figure 9 shows the residue configuration of the multiple protonated states.

### 3.1.3 Conformational Entropy

| System | apo 0.0.0.0 | holo 0.0.0.0 | 1.0.0.0 | 0.1.0.0 | 0.0.1.0 | 0.0.0.1 | 1.1.0.0 | 1.0.1.0 | 0.1.1.0 | 1.1.1.0 | 1.1.1.1 |
|---|---|---|---|---|---|---|---|---|---|---|---|
| $\Delta S_{conf}$ [kJ/mol] | 0 | 0 | 12 | 0.4 | -73 | -22 | -36 | -55 | -17 | -35 | -53 |

Figure 10: Table showing the change in conformational entropy.

The greatest observed change occurred when E293 was protonated. Figure 10 is a table showing a decrease in Conformational Entropy represents an increase in flexibility. However this data requires replication as it is not consistent with previously undertaken Ramachandran and RMSF plots. For example, the protonated state 1.1.1.1 has the third largest conformational entropy difference this cannot be correct as it was shown to be possess steric hindrance features. Therefore, this conformational entropy data must be disregarded and reproduced.

### 3.1.4

Mutual Information

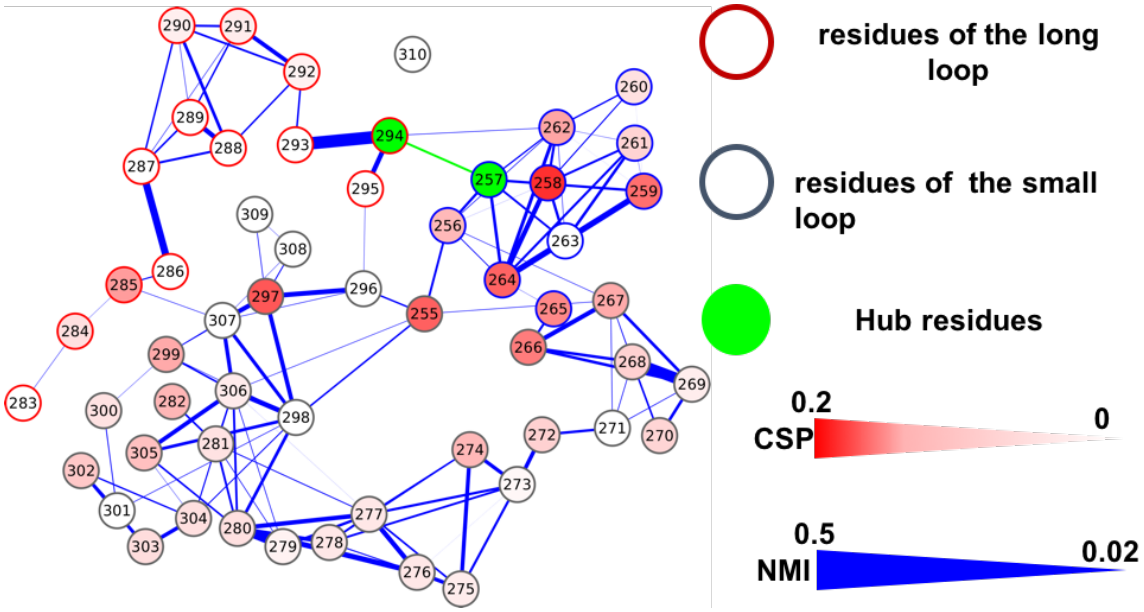


Figure 11: Mutual information network of unprotonated Ca2+ binding site

Figure 11 maps the connectivity of the unprotonated state for Langerin residues. Residues of the long loop are highlighted in red and residues of the small loop are highlighted in blue. Residues 294 and 257 are considered the hub residues and are highlighted in green. The mutual information graphs help determine the effect of protonation upon the connection between the small and long loop, which is crucial in Ca2+ binding. The figure below compares the mutual information of the single protonated states.

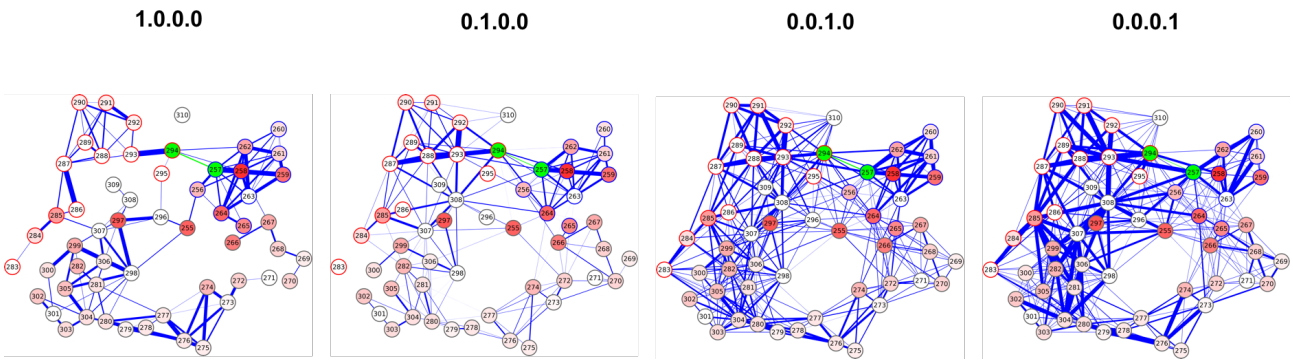


Figure 12: Mutual information network for single protonated states

It can be seen in figure 12 that both E293 and D308 protonation cause a huge increase in connectivity between the hub residues and therefore the two loops. H295 shows little change from unprotonated and E284 shows only a slight increase in connectivity between the loops.

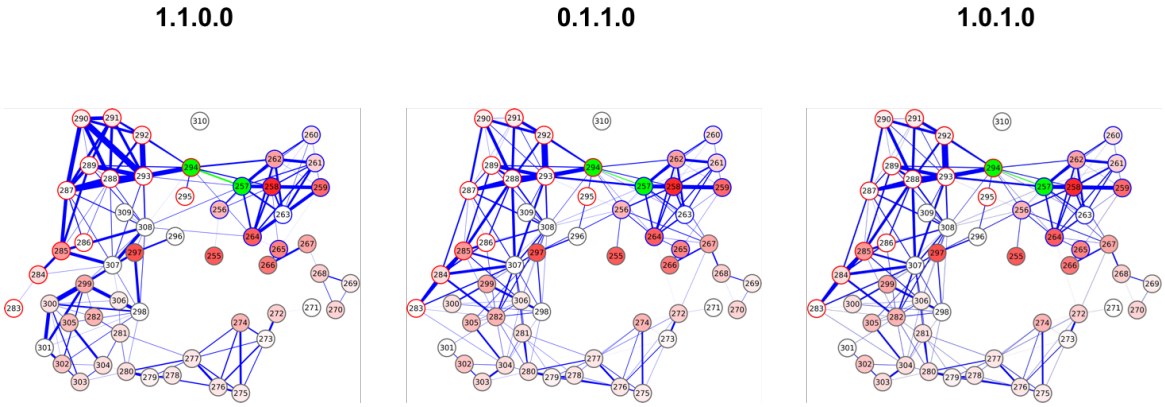


Figure 13: Mutual information network for double protonated states

Upon protonation of both H294 and E285, there is an increase connectivity within the long and small loop no increase in connectivity between the loops occurs. This lack of loop connectivity is also present in the doubly protonated states of E285 and E293 as well as H294 and E293. This suggests that the protonation of these residues together causes loop independence to be energetically favorable.

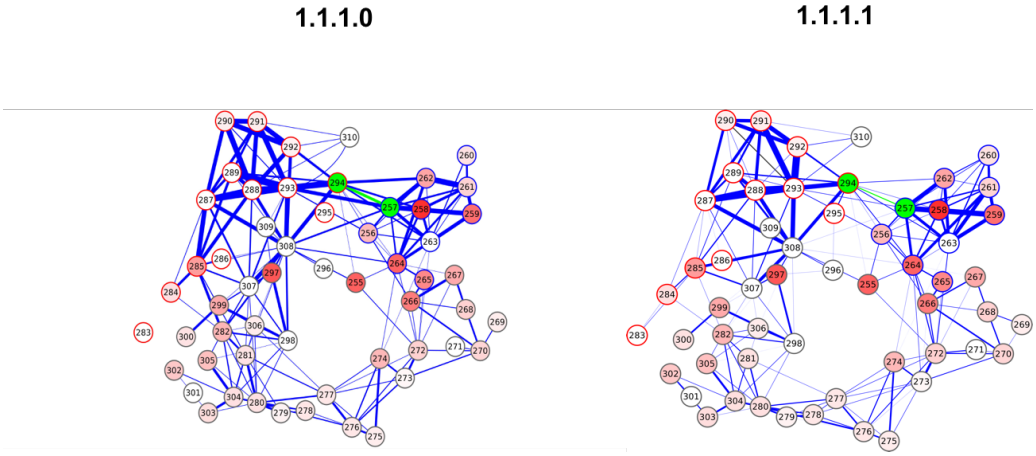


Figure 14: Mutual information network for multiple protonated states

A further increase in connectivity within the loops is observed in the multiple protonation states but still with no increase in connectivity between the two loops.

## 3.2 Hydrogen Bond Analysis

The table below shows the change in bond strength of 16 unique hydrogen bonded residue pairs. The residue pairs were located between the residues of greatest conformational change upon protonation (257 and 308).

| Conserved | . | 0.0.0.0 | 0.0.1.0 | 0.1.0.0 | 1.0.0.0 | 0.0.0.1 | 1.1.0.0 | 1.0.1.0 | 0.1.1.0 | 1.1.1.0 | 1.1.1.1 |
|---|---|---|---|---|---|---|---|---|---|---|---|
| Donor | Acceptor | % | % | % | % | % | % | % | % | % | % |
| N307 Side | N297 Main | 69.66 | 65.4 | 72.22 | 72.62 | 74.83 | | | | 70 | 64.67 |
| N292 Side | A289 Main | 45.65 | 18.59 | 17.06 | 41.48 | 13.37 | | | | | |
| I282 Main | T306 Main | 90.23 | 74.24 | 88.69 | 88.51 | 84.49 | 82.8 | 86.6 | 85.8 | 87.68 | 86.57 |
| G285 Main | I282 Main | 71.79 | | | | | 29.4 | 59.2 | 55.1 | 57 | 41 |
| K299 Main | A305 Main | 88.23 | 66.24 | 66.28 | 89.57 | 68.31 | 65.6 | 78.7 | 70.7 | 74.74 | 64.9 |
| N297 Main | N307 Main | 90 | 89.09 | 88.91 | 89.09 | 87.96 | 89.2 | 88.3 | 90.9 | 90.56 | 91.96 |
| A258 Main | D263 Main | 62.38 | 63.82 | 68.81 | 61.58 | 58.08 | | | | 57.61 | 51.11 |
| G262 Main | G259 Main | 24.6 | | | | | 22.6 | 21.9 | 14.3 | 11.16 | 21.63 |
| A278 Main | L274 Main | 14.26 | 12.56 | 13.96 | 17.63 | 15.49 | 14.2 | 14.7 | 11.7 | | |
| N288 Side | D308 Side | 80.95 | 35.22 | 27.88 | 80.26 | 13.36 | | | | 63.12 | 86.16 |
| N307 Side | N297 Main | 87.64 | 18.5 | 51.74 | 89.76 | 29.38 | | | | 29.62 | 22.09 |
| N291 Main | N288 Side | 34.96 | 13.45 | 30.32 | 34.92 | 23.97 | | | | 97.77 | 64.68 |
| N287 Side | D308 Side | 99.58 | 59.26 | 99.21 | 97.45 | 12.92 | | | | 54.73 | 64.51 |
| K257 Side | H294 Main | 50.38 | 59.98 | 67.81 | 51.94 | 58.73 | | | | 37.08 | 46.78 |
| K274 Side | D263 Main | 45.96 | 32.62 | 41.47 | 42.86 | 29.5 | | | | | |
| G293 Main | N288 Side | 54.11 | | | | | | | | 14.73 | 20.2 |

Figure 15: Table of unique hydrogen bonds for all protonated states

The table seen in figure 15 highlights that greatest changes in hydrogen bond strength is due to the protonation of E293. This is seen in the unique bond between N307 and N297, which drops significantly from 87.64% to 18.5% upon protonation. In addition, the bond strength of N287 and D308 drops from 99.58% to 59.26%. The protonation of H283 states vary very little from the unprotonated state suggesting that this residue has little effect upon the binding site.

## 3.3 Pka Analysis

Figure 16 below shows the pKa values of the 4 key residues in the Ca2+ binding pocket of the Langerin protein. The residue highlighted in red is the residue for which pKa is calculated. The grey highlighted residue shows the residue that has been protonated. White shows the unprotonated residues. $HX \Rightarrow X$ represents the protonated ensemble, while $X \Rightarrow HX$ represents the unprotonated ensemble.

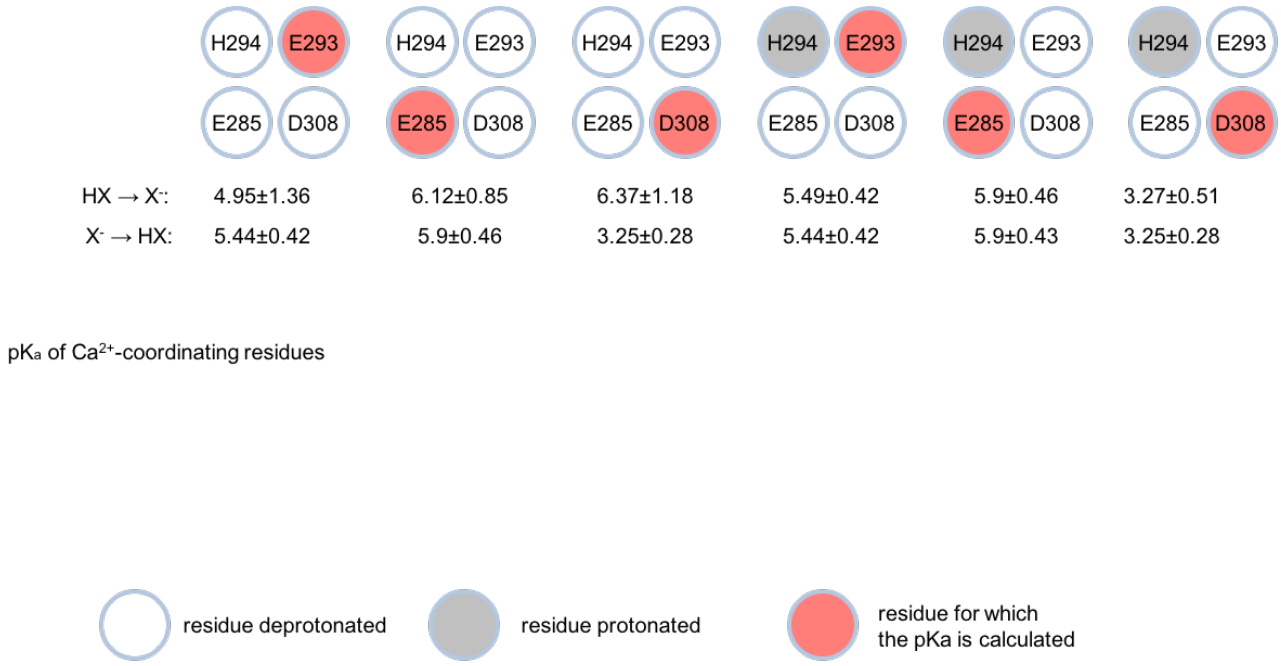


Figure 16: Calculated pKa values for specific residues for single protonated states

From figure 15 it can be seen that the protonation of H294 has little affect on the pKa values of the other Ca2+ binding pocket residues. The protonation and pKa calculation of residue D308 has the greatest change, with a calculated pKa value of 3.25 unprotonated and 6.37 upon protonation. This indicates a more tightly bound structure. E293 shows a significant decrease in pKa value upon protonation. The pKa value drops from 5.44 to 4.95, suggesting a looser bound structure.

## 3.4 Allosteric Network

By comparing the natural log of the correction function (ACF) between the two hub residues for each loop, the time dependent connection between the two binding site loops can be analyzed. The distance between the two residues was also analysed for protonation dependence, represented by the number of time the residues were separated by a certain distance.

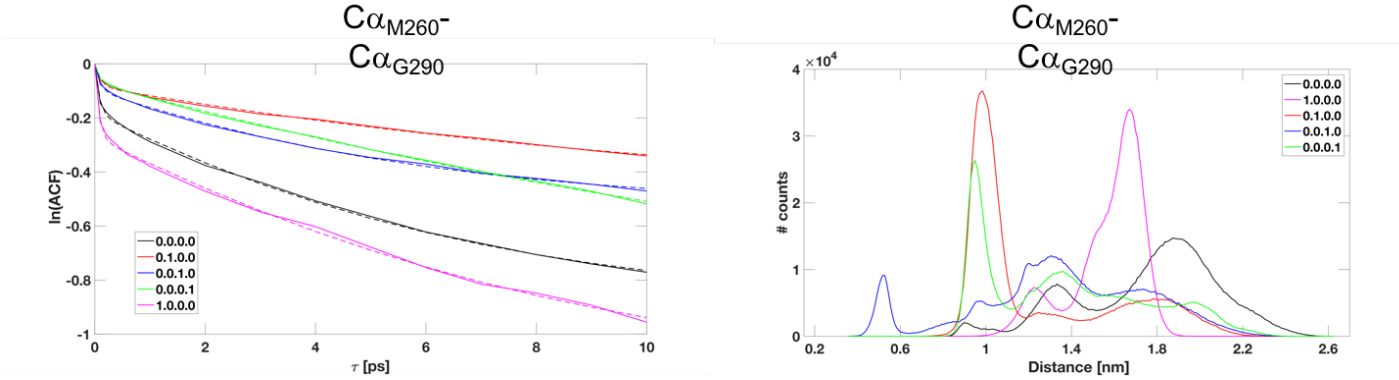


Figure 17: Allosteric network for single protonated states

Figure 17 shows the allosteric transition for the single protonated states. It can be seen that as time progresses over a time scale of picoseconds the correlation between the residues exponentially decreases. The protonation of H294 shows the lowered correlation between the residues, even lower than the unprotonated state. Protonated states D308, E293 and E285 produce consistently more correlation, between M260 and G290, than the unprotonated state.

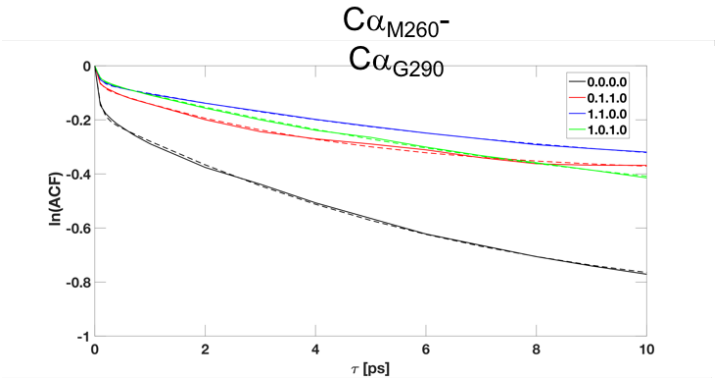


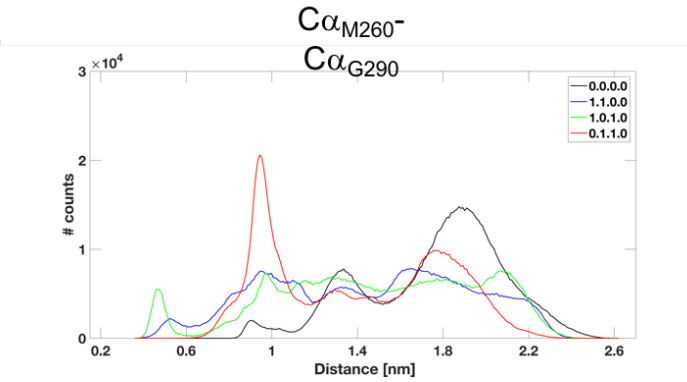


Figure 18: Allosteric network for double protonated states

Figure 18 shows the allosteric transition for the double protonated states. All doubly protonated states produce a stronger connection between the loops than the unprotonated state.

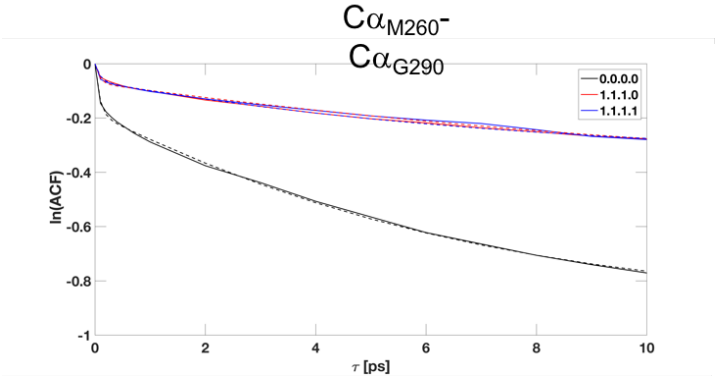


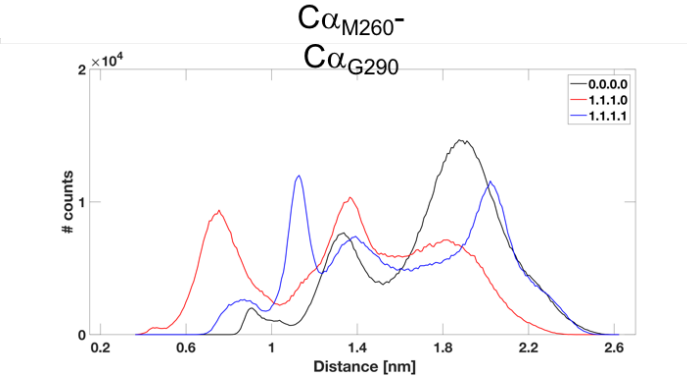


Figure 19: Allosteric network for multiple protonated states

Figure 19 shows the allosteric transition for the multiple protonated states, these produced almost identical time dependence correlation between the hub residues. The figure shows both states to be more correlated than the unprotonated state.

## 3.5 Discussion

Analysis of the results of the protonated states suggests that the residue E293 has the strongest influence on the Ca2+ release. This suggestion comes from the large increase in RMSF, Ramachandran flexibility and mutual information connectivity between the two loops due to E293 protonation. The Hydrogen bond analysis showed that the greatest change in bond strength and therefore bond geometry was due to E293 protonation. pKa analysis also provided evidence of E293 producing a significant decrease in pKa value upon protonation.
The results provide evidence that the coupling between the long and short loop is significantly influenced by the protonation of the residue triad; E285, E293 and D308. This evidence is present in the mutual information networks. Upon protonation of E293, D308 and E285 an increase in connectivity between the two loops is observed. This suggests that these residues are important components to the binding site as the connectivity and coupling of the two loops is crucial for Ca2+ binding.
The data suggest that residue H294 protonation does not cause any major conformational changes to the Ca2+ binding site. This suggestion is consistent in all analysis techniques used in this report and is seen across single, double and multiple protonated states which include H285 protonation.
The conformational entropy analysis used produced redundant results. Before further analysis a thorough replication of the conformational entropy should be preformed in order to support the conclusions of this report.

# 4 Conclusion

The data suggests that a protonation of a single residue in the long loop does indeed introduces a huge conformational changes in the long loop. The data showed that the pH dependent component is encoded in the triad E285, E293, D308. Coupling of the long and short loop is stronger in triad protonated states than in unprotonated, and H295 systems. Huge perturbations of the Hydrogen bond network were observed upon protonation, indicating a strong relationship between the conformation and the hydrogen bond network.

# References


[1] Munoz-Garcia JC, Chabrol E, Vives RR, Thomas A, De Paz JL, Rojo J, et al. Langerin–Heparin Interaction: Two Binding Sites for Small and Large Ligands As Revealed by a Combination of NMR Spectroscopy and Cross-Linking Mapping Experiments. Journal of the American Chemical Society. 2015;137(12):4100–4110.

[2] Feinberg H, Powlesland AS, Taylor ME, Weis WI. Trimeric structure of langerin. Journal of Biological Chemistry. 2010;285(17):13285–13293.

[3] Zelensky AN, Gready JE. The C-type lectin-like domain superfamily. Febs Journal. 2005;272(24):6179–6217.

[4] Valladeau J, Ravel O, Dezutter-Dambuyant C, Moore K, Kleijmeer M, Liu Y, et al. Langerin, a novel C-type lectin specific to Langerhans cells, is an endocytic receptor that induces the formation of Birbeck granules. Immunity. 2000;12(1):71–81.

[5] de Witte L, Nabatov A, Pion M, Fluitsma D, De Jong MA, de Gruijl T, et al. Langerin is a natural barrier to HIV-1 transmission by Langerhans cells. Nature medicine. 2007;13(3):367–371.

[6] Hanske J, Aleksic S, Ballaschk M, Jurk M, Shanina E, Beerbaum M, et al. Intradomain Allosteric Network Modulates Calcium Affinity of the C-Type Lectin Receptor Langerin. Journal of the American Chemical Society. 2016;138(37):12176–12186.

[7] Fuglebakk E, Echave J, Reuter N. Measuring and comparing structural fluctuation patterns in large protein datasets. Bioinformatics. 2012;28(19):2431–2440.

[8] Berg JM, Tymoczko JL, Stryer L. Biochemistry: international edition. WH Freeman: New York, NY, USA; 2006.

[9] Cooper J. The Ramachandran Plot; 1995. Accessed: 2016-11-12. `http://www.cryst.bbk.ac.uk/PPS95/course/3_geometry/rama.html`.

[10] Vu PM. Lecture 1: Entropy and mutual information;. Available from: `http://www.ece.tufts.edu/ee/194NIT/lect01.pdf`.

[11] Hubbard RE, Kamran Haider M. Hydrogen bonds in proteins: role and strength. eLS. 2010;.

[12] gromacs. gmx bond;. Available from: `http://manual.gromacs.org/programs/gmx-hbond.html`.

[13] Shimadzu - analytical and measurement instruments;.

[14] Di Russo NV, Estrin DA, Martí MA, Roitberg AE. pH-Dependent Conformational Changes in Proteins and Their Effect on Experimental pK as: The Case of Nitrophorin 4. PLoS Comput Biol. 2012;8(11):e1002761.

[15] Reijenga J, Van Hoof A, Van Loon A, Teunissen B. Development of methods for the determination of pKa values. Analytical chemistry insights. 2013;8:53.

[16] Alexov E, Mehler EL, Baker N, M Baptista A, Huang Y, Milletti F, et al. Progress in the prediction of pKa values in proteins. Proteins: structure, function, and bioinformatics. 2011;79(12):3260–3275.

[17] Dokholyan NV. Controlling allosteric networks in proteins. Chemical reviews. 2016;.